Experimental and numerical analyses of high voltage 4H-SiC junction barrier Schottky rectifiers with linearly graded field limiting ring*

Wang Xiang-Dong(王向东)[a], Deng Xiao-Chuan(邓小川)[a]†, Wang Yong-Wei(王永维)[b], Wang Yong(王 勇)[b], Wen Yi(文 译)[a], and Zhang Bo(张 波)[a]

[a] *State Key Laboratory of Electronic Thin Films and Integrated Devices, University of Electronic Science and Technology of China, Chengdu* 610054, *China*
[b] *National Key Laboratory of ASIC, Shijiazhuang* 050051, *China*

(Received 29 July 2013; revised manuscript received 20 November 2013; published online 25 March 2014)

This paper describes the successful fabrication of 4H-SiC junction barrier Schottky (JBS) rectifiers with a linearly graded field limiting ring (LG-FLR). Linearly variable ring spacings for the FLR termination are applied to improve the blocking voltage by reducing the peak surface electric field at the edge termination region, which acts like a variable lateral doping profile resulting in a gradual field distribution. The experimental results demonstrate a breakdown voltage of 5 kV at the reverse leakage current density of 2 mA/cm^2 (about 80% of the theoretical value). Detailed numerical simulations show that the proposed termination structure provides a uniform electric field profile compared to the conventional FLR termination, which is responsible for 45% improvement in the reverse blocking voltage despite a 3.7% longer total termination length.

Keywords: 4H-SiC, junction barrier Schottky rectifier, linearly graded field limiting ring, breakdown voltage

PACS: 72.20.Ht, 73.30.+y, 85.30.Mn **DOI:** 10.1088/1674-1056/23/5/057203

1. Introduction

Silicon carbide (SiC) is considered to be an excellent material for high power and high temperature semiconductor applications due to its superior properties of a high critical electric field and high thermal conductivity.[1,2] Until now, a large number of SiC junction barrier Schottky (JBS) rectifiers have been reported for a wide range of applications.[3–5] The main advantages of the JBS rectifier are the Schottky-like on-state and the fast switching characteristics together with the off-state characteristics having a low leakage current similar to that of the PiN rectifier. To reach a breakdown voltage close to the ideal one, various junction termination techniques for the SiC devices have been developed, involving field plate (FP),[6] field limiting ring (FLR),[7] and single- and multiple-junction termination extensions (JTE).[8–10] Among all of those edge termination structures, the FLR termination has been used extensively for high voltage SiC JBS rectifiers since it is usually formed simultaneously with the main junctions, thus saving costly processing steps. However, this method for the SiC devices is strongly dependent on the ring spacing of FLR due to the relatively shallow junction depth, which correlates closely to the critical characteristics of the breakdown voltage for SiC JBS rectifiers.[11] Consequently, the spacing and the width of the rings need careful design for the maximum breakdown voltage with minimal area consumption.

In this paper, an experimental work on the fabrication and electrical characterization of 4H-SiC JBS rectifiers with a linearly graded field limiting ring (LG-FLR) is presented. Experimental and simulation results show that the proposed structure with 5 kV blocking capability has a prominent improvement in the breakdown voltage characteristics compared to those rectifiers with the conventional FLR. The experimental breakdown voltages obtained on the 4H-SiC JBS rectifiers with LG-FLR structure are compared with the simulation data.

2. Physical models

In this paper, the two-dimensional numerical device characteristics are simulated with Atlas from Silvaco.[12] The details of the models are taken from the most recent literature. The key physical models used in the simulation include the models for mobility, carrier generation–recombination, incomplete ionization of impurities, impact ionization, and bandgap.

The mobility of the carriers in 4H-SiC is modeled using the Caughey–Thomas expression, which is used to specify the doping- and temperature-dependent low field mobility[13]

$$\mu_{\mathrm{n,p}} = \mu_{0\mathrm{n,p}}^{\min}\left(\frac{T}{300}\right)^{\alpha_{\mathrm{n,p}}} + \frac{\mu_{0\mathrm{n,p}}^{\min}(T/300)^{\beta_{\mathrm{n,p}}} - \mu_{0\mathrm{n,p}}^{\min}(T/300)^{\alpha_{\mathrm{n,p}}}}{1+\left(N/N_{\mathrm{n,p}}^{\mathrm{crit}}\right)^{\gamma_{\mathrm{n,p}}}}, \quad (1)$$

where N is the total impurity concentration, and $N_{\mathrm{n,p}}^{\mathrm{crit}}$ is the doping concentration at which the mobility is halfway between

*Project supported by the State Key Program of the National Natural Science Foundation of China (Grant No. 61234006).
†Corresponding author. E-mail: xcdeng@uestc.edu.cn
© 2014 Chinese Physical Society and IOP Publishing Ltd

the min and the max values (i.e, the mobilities in highly doped and undoped materials, respectively). Both $\mu_{0n,p}^{min}$ and $\mu_{0n,p}^{max}$ are the mobilities at room temperature.[14] Terms $\alpha_{n,p}$, $\beta_{n,p}$, and $\gamma_{n,p}$ are the fitting coefficients.

The velocity saturation at high electric fields is modeled with the Canali model

$$\mu_{n,p}(E) = \frac{\mu_{n_0,p_0}}{\left(1+\left(\mu_{n0,p0}E/\upsilon_{sat}\right)^{\beta_E}\right)^{1/\beta_E}}. \quad (2)$$

Here, E is the parallel electric field, β_E is the fitting coefficient, and μ_{n0} and μ_{p0} are the low field electron and hole mobilities, respectively.

The effect of the recombination centers can be described by the conventional Shockley–Read–Hall (SRH) recombination/generation expression[15,16]

$$R_{SRH} = \frac{np - n_i^2}{\tau_p\left(n + n_i\exp\left(E_{trap} - E_C\right)\right) + \tau_n\left(p + n_i\exp\left(E_V - E_{trap}\right)\right)}, \quad (3)$$

where

$$\tau_{n,p} = \frac{\tau_{n0,p0}}{1+\left(N/N_{n,p}\right)}. \quad (4)$$

Here, τ_n and τ_p are the electron and hole lifetimes, respectively, n_i is the effective intrinsic carrier concentration, n and p are the electron and hole densities, respectively, E_{trap} is the difference between the trap energy level and the intrinsic Fermi level, and N_n and N_p are the characteristic parameters for electrons and holes, respectively.

The description of the impact ionization, which is critical to the simulation of blocking characteristics, adopts the Selberherr model[17]

$$\alpha_{n,p} = a_{n,p}\exp\left(-\frac{b_{n,p}}{E}\right). \quad (5)$$

Here, E is the electric field in the direction of the current flow at a particular position in the structure, and parameters $a_{n,p}$ and $b_{n,p}$ are fitting coefficients.[18,19]

3. Device fabrication

Figure 1 shows a cross-sectional view of the fabricated 5 kV 4H-SiC SiC JBS rectifier with LG-FLR structure. The layer structure consists of an N^+, 8° off-axis 4H-SiC substrate purchased from Cree, Inc., followed by two n-type epitaxial layers. The first epi-layer is 30 μm thick with a doping concentration of 2×10^{15} cm^{-3}. The second layer is 20 μm thick with a doping concentration of 2.5×10^{15} cm^{-3}. Next, the P^+ implanted field limiting rings at the periphery of the JBS rectifier and the stripe patterns of p-type grids within the active JBS rectifier area were formed simultaneously by multiple aluminum ion implantations having a box profile. The peak concentration and the depth of the P^+ implantations are 5×10^{18} cm^{-3} and 0.5 μm, respectively. The active area and the total area of each device are 0.09 mm^2 and 1.5 mm^2, respectively. The activation annealing of all implanted regions was carried out simultaneously at 1600 °C for 30 min without a capping layer in Ar ambient. A Ni(200 nm)/Au(500 nm) double layer was used as the backside metal followed by annealing at 1000 °C in Ar ambient for 2 min to form the cathode Ohmic contact. Subsequently, the triple layer metallization of Ni(150 nm)/Ti(350 nm)/Au(600 nm) was used to form the Schottky contact to the N^- epitaxy followed by annealing at 500 °C in Ar ambient for 5 min. Finally, a SiO_2 layer was deposited as a passivation layer.

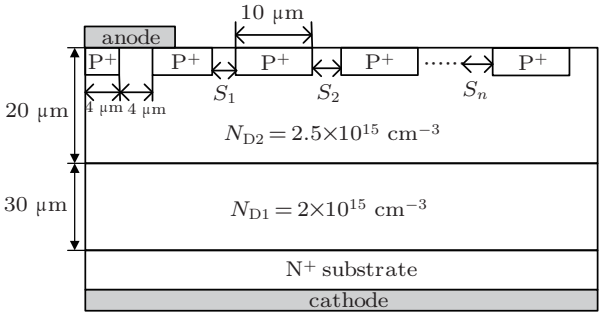


Fig. 1. Schematic cross-section of a 4H-SiC JBS rectifier with 35-ring LG-FLR termination.

A photograph of the fabricated 4H-SiC JBS rectifier is presented in Fig. 2. As shown in Fig. 1, the p-type grid layout of the stripe structure for JBS is designed with a width of 4 μm and a spacing of 4 μm between them. The width of the P^+ implanted field limiting ring is 10 μm. The spacing between the P^+ implantation rings ($S_{4,\ldots,35}$) linearly increases from 2 μm to 5.1 μm with the first four spacings ($S_{1,2,3,4}$) keeping constant, in order to effectively separate the linearly graded spacing structure from the central active region.

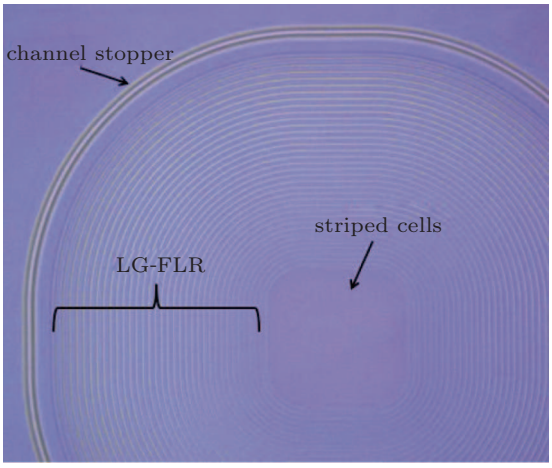


Fig. 2. (color online) Photograph of the fabricated 4H-SiC JBS rectifier with 35-ring LG-FLR termination.

The linearly graded spacings between adjacent rings induce the gradual decrease of the effective charge in the FLR regions, which results in a gradual and smooth field distribution across the termination region. To understand the origin

of the variation of the effective doping concentration, the normalized effective doping factor (α) is defined as

$$\alpha = \frac{N_n}{N_1}, \tag{6}$$

$$N_n \times S_n = N_1 \times S_1, \tag{7}$$

where N_n and S_n are the effective doping concentration and the spacing at each ring of LG-FLR, respectively. The normalized effective doping factor at each ring for the LG-FLR structure is shown in Fig. 3. It is seen that the effective lateral doping profile of the overall FLR region can be realized by applying the variable ring spacings.

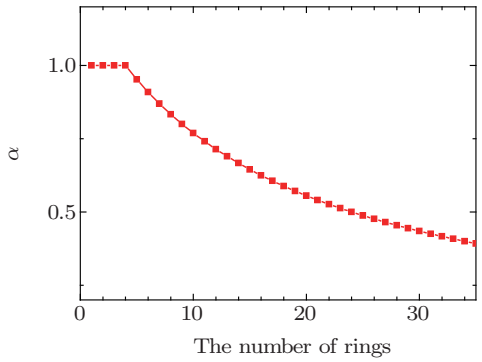


Fig. 3. (color online) Normalized effective doping factor at each ring in the 35-ring LG-FLR.

4. Results and discussion

Both the experimental forward and reverse characteristics on an individually packaged SiC JBS rectifier were measured using an Agilent B1505 semiconductor parameter analyzer. Figure 4 shows the experimental and the simulated forward *J*–*V* characteristics of the fabricated 4H-SiC JBS rectifier at room temperature. It is demonstrated that the Schottky contact turns on at the forward voltage of 1.15 V with the specific on-resistance of 349 mΩ·cm^2. When the forward voltage exceeds 2.5 V, the current increases rapidly with the increasing forward voltage due to the bipolar current injection from the P+ grids. The large specific on-resistance is ascribed to the poor 4H-SiC surface roughness resulting from the high temperature activation annealing without effective surface protection, leading to the non-uniform Schottky conduction. This phenomenon has been predicted by introducing traps into Atlas simulation models, which also predict the conduction modulation with the anode metal and the P$^+$ region set as Ohmic contacts in the simulation.

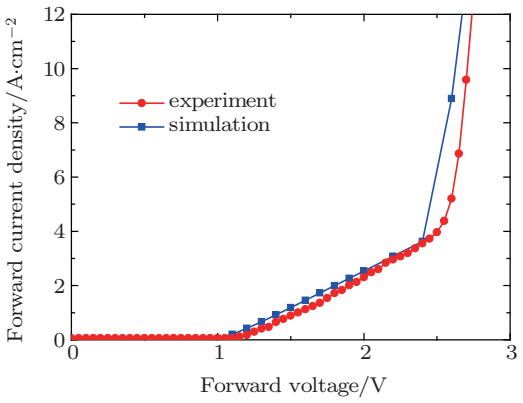


Fig. 4. (color online) Experimental and simulated forward *J*–*V* characteristics of the fabricated 4H-SiC JBS rectifier.

Figure 5 shows the experimental reverse *J*–*V* characteristic of the fabricated 4H-SiC JBS rectifier with a 35-ring LG-FLR at room temperature. The breakdown voltage of the proposed structure is over 5 kV when the leakage current density is 2 mA/cm^2, which approaches 80% of the ideal parallel plane breakdown voltage. The simulated potential contours of the LG-FLR structure in off-state are shown in Fig. 6. It is shown that the potential contours are distributed regularly in the edge termination region at the breakdown voltage of 6 kV. The guard ring structure serves to reduce the amount of field crowding at the main junction by spreading the depletion region past floating junctions with consecutively lower potential. As can be observed from the figure, the depletion region of the LG-FLR structure only spreads laterally to the 28th ring. This is mainly due to the fact that the 35-ring LG-FLR structure was adopted to reduce the impact of the manufacturing process on the breakdown voltage, although the optimized number of field limiting rings for maximum breakdown is around 28 in the numerical simulations.

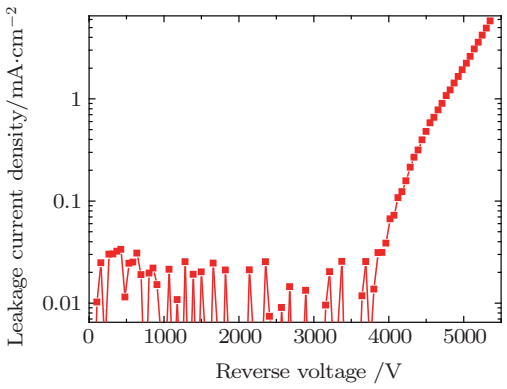


Fig. 5. (color online) Experimental reverse *J*–*V* characteristic of the 4H-SiC JBS rectifier with 35-ring LG-FLR termination.

Figure 7 illustrates the comparison of the simulated reverse breakdown characteristics of the proposed structure and the conventional FLR structures with constant spacings of 2 μm and 3 μm, whose total termination lengths (L_{FLR}) are 470 μm, 420 μm, and 455 μm, respectively. In this work, the breakdown voltage of the 4H-SiC JBS rectifier is determined when the reverse leakage current exceeds 1×10^7 A/μm. On the other hand, in order to concentrate on the pure effect of the proposed LG-FLR structure, materials and interfaces are ideally free from oxide charges in the passivation layers and traps at the anode interface, which is responsible for the difference

between the simulated breakdown voltage and the measured breakdown voltage. It is found that the blocking voltage is 3.9 kV ($S_{1-35\text{rings}} = 3$ μm) and 4.2 kV ($S_{1-35\text{rings}} = 2$ μm) for the SiC JBS rectifiers with conventional FLR structures but is increased by 45% to 6.1 kV by applying the LG-FLR structure. This improvement in breakdown voltage is considered to be caused by the linearly variable ring spacings, resulting in the gradual equivalent concentration in the LG-FLR termination region. According to the Poisson equation, a lower concentration results in a smaller slope of the electric field, leading to a gradual and smooth field distribution. Figure 8 shows the surface electric field distributions at breakdown for the 35-ring FLR termination with different ring spacings. As can be observed, by introducing the LG-FLR structure, the extremely flat electric field distribution across the termination region can be obtained. As mentioned above, actually 28 rings are adequate for the LG-FLR structure, resulting in the breakdown voltage of 6.1 kV at the expense of L_{FLR} of 436 μm. However, the maximum surface electric field is found at the outer edge and the inner side of the terminations for conventional 2 μm- and 3 μm-spacing FLR structures, respectively, which leads to the premature breakdown. Particularly, the electric field of the 3 μm-spacing case approximates zero at the 28th ring, implying that further increase of the rings does not help improve the breakdown voltage. Moreover, the conventional 2 μm-spacing FLR structure fully utilizes its termination length, which is 3.7% shorter than that of the LG-FLR, but it achieves 31% lower breakdown voltage.

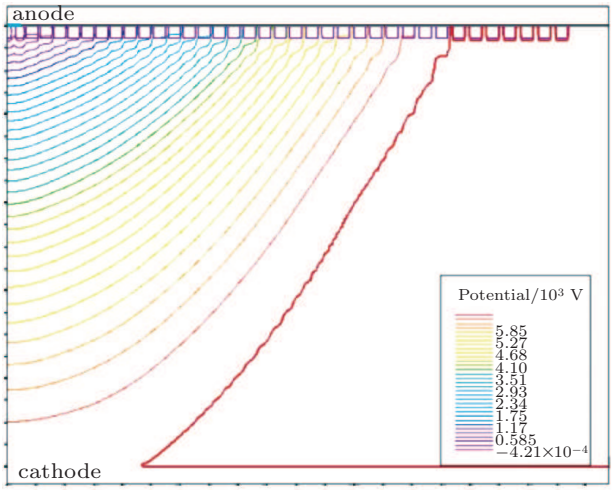


Fig. 6. (color online) Potential contours in off-state of the 4H-SiC JBS rectifier with 35-ring LG-FLR termination.

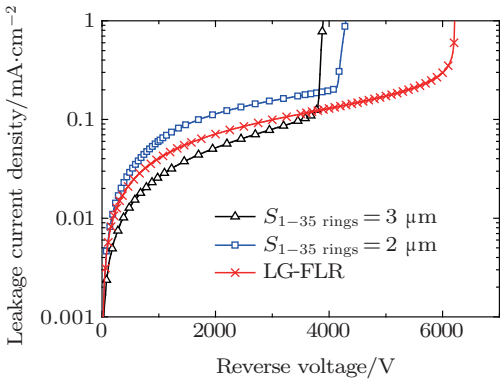


Fig. 7. (color online) Simulated reverse *J*–*V* characteristics for LG-FLR structure and conventional FLR structures with constant spacings of 2 μm and 3 μm.

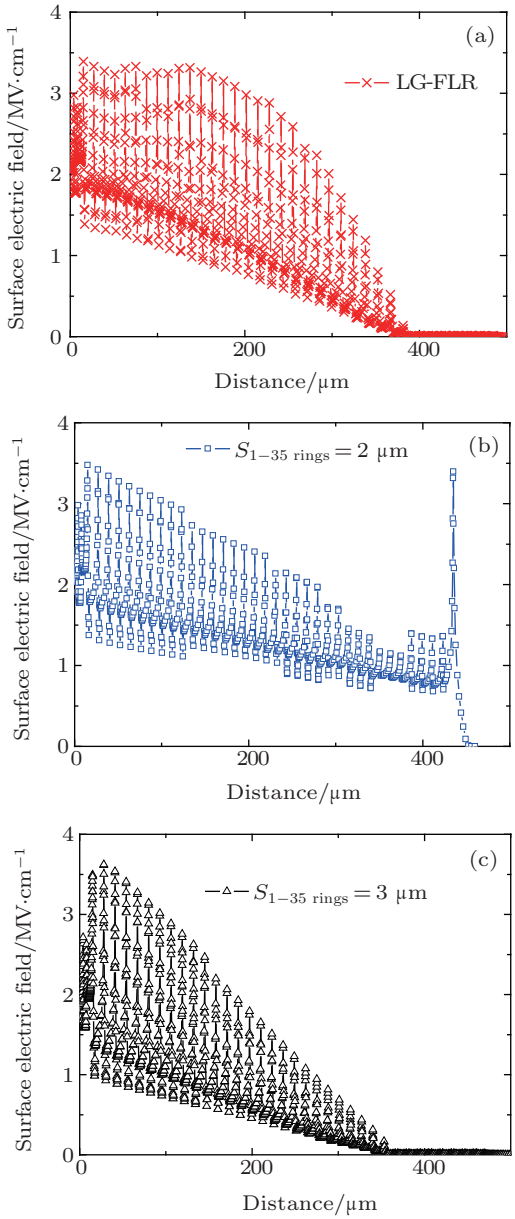


Fig. 8. (color online) Surface electric field distributions at breakdown of (a) LG-FLR termination and conventional FLR terminations with constant spacings of (b) 2 μm and (c) 3 μm.

To determine the optimum LG-FLR termination, the dependence of the breakdown voltage on the number of rings is demonstrated in Fig. 9. It is obvious from this graph that the number of rings has a significant effect on the breakdown voltage. The breakdown voltage of the SiC JBS rectifier increases with the increasing number of rings till 28 and later remains the same with further increase in rings. With the number of

rings increasing to 28, the electric field peak becomes lower at the last ring and more uniform at the inner rings until a uniform electric field distribution is obtained across all 28 rings. Any further increase in the number of rings does not change the electric field distribution and the breakdown voltage because the depletion region does not extend to those rings. Therefore, the approximately constant blocking voltage region represents the efficiency of the edge termination with respect to the maximum blocking voltage capability for the designed electric field distribution across each ring.

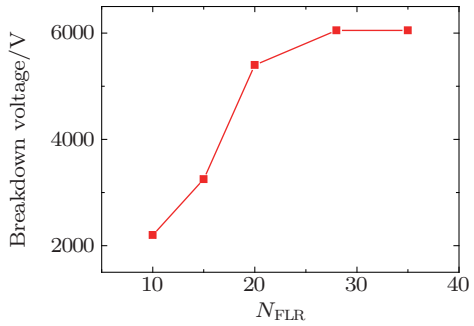


Fig. 9. (color online) The variation in the breakdown voltage with the number of rings of the LG-FLR termination.

5. Conclusion

In this work, a 5-kV 4H-SiC JBS rectifier with a linearly graded FLR termination structure is successfully developed. Simulated results show that the reverse breakdown voltage increases from 4.2 kV to 6.1 kV by applying the linearly variable ring spacings to the conventional FLR structure despite a 3.7% longer total termination length. This improvement in the blocking voltage is attributed to the linearly variable ring spacings, which induce the gradual equivalent concentration in the termination region of the proposed device, thus resulting in a uniform electric field profile across all rings. These results indicate that the 4H-SiC JBS rectifier with LG-FLR is promising as a high-voltage operation device for high-power switching applications.

References

[1] Ning P Q, Zhang D, Lai R X, Jiang D, Wang F, Boroyevich D, Burgos R, Karimi K, Immanuel V D and Solodovnik E V 2013 *IEEE Industrial Electronics Magazine* **7** 6
[2] Qin H H, Zhao B, Nie X, Wen J P and Yan Y G 2013 *8th IEEE Conference on Industrial Electronics and Applications* p. 466
[3] Duong T H, Hefner A R and Hobart K D 2012 *IEEE Energy Conversion Congress and Exposition* p. 4274
[4] Singh R and Sundaresan S 2013 *28h Annual IEEE Applied Power Electronics Conference and Exposition* p. 226
[5] Lentijo K and Hobart K 2013 *IEEE Electric Ship Technologies Symposium* p. 162
[6] Chen F P, Zhang Y M, Zhang Y M, Lü H L and Song Q W 2010 *Chin. Phys. B* **19** 047305
[7] Zhang F S and Li X R 2011 *Chin. Phys. B* **20** 067102
[8] Bolotnikov A V, Muzykov P G, Zhang Q C, Agarwal A K and Sudarshan T S 2010 *IEEE Trans. Electron. Dev.* **57** 1930
[9] Sung W, Brunt E V, Baliga B J and Huang A Q 2011 *IEEE Electron Dev. Lett.* **32** 880
[10] Feng G, Suda J and Kimoto T 2012 *IEEE Trans. Electron. Dev.* **59** 414
[11] Sheridan D C, Niu G, Merrett J N, Cressler J D, Ellis C and Tin C 2000 *Solid-State Electron.* **44** 1367
[12] Http://www.silvaco.com/products/device_simulation/atlas.html [2013-7-20]
[13] Caughey D M and Thomas R E 1967 *Proc. IEEE* **55** 2192
[14] Yoder M N 1996 *IEEE Trans. Electron. Dev.* **43** 1633
[15] Hall R N 1952 *Phys. Rev.* **87** 387
[16] Shockley W and Read W T 1952 *Phys. Rev.* **87** 835
[17] Overstraeten V R and De M H 1970 *Solid-State Electron.* **13** 583
[18] Raghunathan R and Baliga B J 1999 *Solid-State Electron.* **43** 199
[19] Zhao J H, Gruzinskis V, Luo Y, Weiner M, Pan M, Shiktorov P and Starikov E 2000 *Semicond. Sci. Technol.* **15** 1093